



# Unsaturated zone model complexity for the assimilation of evapotranspiration rates in groundwater modeling

Simone Gelsinari<sup>1,2</sup>, Valentijn R.N. Pauwels<sup>1</sup>, Edoardo Daly<sup>1</sup>, Jos van Dam<sup>3</sup>, Remko Uijlenhoet<sup>4</sup>, and Rebecca Doble<sup>2</sup>

<sup>1</sup>Department of Civil Engineering, Monash University, Clayton, Victoria, Australia

<sup>2</sup>CSIRO Land and Water, Waite Campus, Glen Osmond, South Australia, Australia

<sup>3</sup>Soil physics and Land Management, Wageningen University & Research, Wageningen, The Netherlands

<sup>4</sup>Hydrology and Quantitative Water Management Group, Wageningen University & Research, Wageningen, The Netherlands

**Correspondence:** Simone Gelsinari (simone.gelsinari@monash.edu)

**Abstract.** The bio-physical processes occurring in the unsaturated zone have a direct impact on the water table dynamics. Representing these processes through the application of Unsaturated Zone Models (UZMs) of different complexity can have an impact on the estimates of recharge rates. In coupled configurations with UZMs, these recharge rates are often used as input for groundwater models and drive the water table dynamic. Because recharge estimates are always affected by uncertainty, model-data fusion methods, such as data assimilation, can be used to reduce the uncertainty in the model results. In this study, the required complexity (i.e. conceptual versus physically-based) of the unsaturated zone model to update groundwater models through the assimilation of evapotranspiration (ET) rates is assessed for a water-limited site in South Australia. ET rates are assimilated because they have been shown to be related to the groundwater table dynamics, and thus form the link between remote sensing data and the deeper parts of the soil profile. It has been found that, under the test site conditions, a conceptual UZM can be used to improve groundwater model results through the assimilation of ET rates.

*Copyright statement.* None

## 1 Introduction

Evapotranspiration (ET) and recharge to the water table (WT) are two major components of the water cycle. Because ET is a function of the soil water content within the root zone, as the root water uptake is distributed along the entire root system (Grinevskii, 2011; Neumann and Cardon, 2012), improving ET estimates, by means of a detailed modeling of the soil water transport, can lead to better simulation of recharge and WT dynamics. This is particularly important when the WT is within the reach of the roots, as it is common in Australian semi-arid catchments (Banks et al., 2011), where the direct transpiration from the WT is a major contribution to the total ET (Mensforth et al., 1994; Orellana et al., 2012).



20 ET is often simulated through numerical models that reproduce the soil water-vegetation interaction. Advanced integrated  
surface water-groundwater models (e.g. Hydrogeosphere (Therrien et al., 2006), CATHY (Camporese et al., 2010), PARFLOW  
Jones and Woodward (2001)) or coupled saturated-unsaturated zone models (Facchi et al., 2004; Simunek et al., 2009; Zhu  
et al., 2012; Van Walsum and Veldhuizen, 2011; Grimaldi et al., 2015) are able to account for the direct groundwater-vegetation  
interaction. In general, the representation of the unsaturated zone is obtained with simple conceptual water balance models or  
25 detailed physically-based models.

Conceptual unsaturated zone models (UZMs) simplify the processes occurring in the unsaturated zone, and are widely used  
for spatially distributed hydrological simulations (Teuling and Troch, 2005). An example is Batelaan and De Smedt (2007),  
who successfully applied a coupled surface-groundwater balance model at the regional scale focusing on the assessment of  
30 recharge rates. Conceptual water balance models have been found to be flexible as they usually require shorter run times and  
fewer parameters, and are suitable when stochastic simulations based on Monte-Carlo techniques are applied (Kim and Stricker,  
1996; Fatichi et al., 2016). However, for more detailed simulations, such as in ecohydrology or agricultural modeling, simple  
UZMs may fail to accurately simulate important processes (i.e. water stress, root growth) (Krysanova and Arnold, 2008), and  
physically-based models are preferred. These models commonly solve the Richards equation for water flow in porous media,  
35 relying on the relationship between volumetric water content, hydraulic conductivity and soil water pressure head (van Dam  
et al., 2008; Scheerlinck et al., 2009). Therefore, physically-based models have the ability to account for specific effects (e.g.  
capillary rise) that affect the calculation of ET, thus impacting recharge estimates. The latter is particularly important when  
UZMs are coupled to saturated models as recharge acts as the link between both models (Doble et al., 2017).

40 Because of the number and spatial variability of parameters (e.g. the water retention curve, detailed vegetation characteris-  
tics) required by physically-based models, their application, particularly in data scarce areas, can be challenging (Simmons and  
Meyer, 2000). On the other hand, conceptual models may require fewer input data, but their recharge estimates may be less  
reliable. This is because they are affected by both structural uncertainty, induced by the simplification of the model (Renard  
et al., 2010), and the epistemic and aleatory uncertainty of the forcing inputs (Khatami et al., 2019). Accurate model parameters  
45 and meteorological inputs are far from always available, especially at large spatial scales. Therefore, the use of remote sens-  
ing data can provide vital information for these models (Entekhabi and Moghaddam, 2007; Carroll et al., 2015; Lu et al., 2020).

One way to make use of the remote sensing observations is through data assimilation, which is a method to combine model  
results with independent observations to reduce model uncertainty. There is a plethora of studies on the assimilation of di-  
50 verse observations (e.g. soil moisture (SM), leaf area index, streamflow and groundwater levels) in hydrology, reviewed several  
times in the last decade by various authors (Liu et al., 2012; Li et al., 2016). Many of these studies are based on satellite re-  
mote sensing data, which have been proven to be a valid alternative when field-based observations cannot provide sufficiently  
accurate measurements. Remotely sensed SM values are a function of the water content of the upper few centimeters of the  
soil (Pipunic et al., 2014). Consequently, models using remotely sensed SM assimilation extrapolate the update for the upper



55 soil layer to the entire modeled soil column through the covariance between the upper and lower layer modeled SM values. On  
the other hand, remotely sensed evapotranspiration rates are a function of the modelled water content of the soil column up to  
the rooting depth. Remotely sensed ET assimilation thus directly updates the water content of the entire modeled soil column.  
In recent years, the assimilation of satellite-based ET observations has been recognized to be beneficial for the reduction of the  
uncertainty of several hydrogeological products (e.g. recharge and depth to WT), especially for data-scarce areas (Entekhabi  
60 and Moghaddam, 2007; Doble et al., 2017; Gelsinari et al., 2020)).

However, all satellite observations present a trade-off between accuracy, time-frequency and spatial coverage, and satellite  
retrievals are not free from errors. For instance, Long et al. (2014) analyzed and compared the uncertainty in the ET esti-  
mates from different sources including the Moderate-Resolution Imaging Spectroradiometer (MODIS). They concluded that  
65 ET derived from land surface models had a lower uncertainty than the MODIS based ET (5 mm/month vs 12.5 mm/month,  
respectively), and suggested a hybrid approach for taking advantage of the integration of land surface models and remotely  
sensed products to reduce uncertainty. Droogers et al. (2010), using a physically-based UZM, applied an inverse modeling  
approach (i.e. forward-backwards optimization), and found that improvements were obtained when the frequency of the ET  
observations was higher than a 15-day interval. Therefore, an assimilation algorithm that correctly accounts for the observation  
70 errors when assimilating remotely sensed ET observations into UZMs should be used for this purpose. This was synthetically  
shown by Gelsinari et al. (2020) who used the Ensemble Kalman Filter (EnKF) for the sequential assimilation of the averaged  
8-days ET into a conceptual UZM coupled to MODFLOW (Harbaugh, 2005), improving the model outputs. Unlocking the po-  
tential of using ET observations to inform models, with the aim of reducing the uncertainty in the outputs, is a currently active  
area of research. The assimilation of satellite ET observations have been shown to be a feasible way to constrain hydrologic  
75 models, but has yet to be validated against experimental data. Furthermore, it is known that UZMs of different complexity can  
yield different ET estimates, producing distinct recharge values and, in turn, a diverse dynamics of the WT.

This study aims to perform the validation of the ET assimilation framework proposed synthetically in Gelsinari et al. (2020)  
and to assess the UZM complexity required for the assimilation to positively update groundwater models. In particular, the  
80 quantities of interest are the temporal WT fluctuation dynamic and the modeled actual ET. A conceptual and a physically-  
based UZM are coupled to MODFLOW, and applied to a water-limited study site in the south-east of South Australia. Remotely  
sensed ET observations are assimilated into both these coupled models, and an assessment of the improvements in the model  
results is made. Based on this assessment, a number of recommendations regarding the required UZM complexity to obtain a  
positive impact on the quantities of interest are made.



## 85 2 Methods

### 2.1 Study Area and Data

The study area is situated in the south-eastern part of South Australia, north of the city of Mount Gambier (See figure 1[a],[b]). This region has a Mediterranean climate, with cool wet winters and warm dry summers. Climatic forcing inputs are rainfall and potential ET (PET) obtained from the Bureau of Meteorology (BOM) station number 26021. The historical data for this station report an average annual rainfall and potential ET of approximately 710 and 980 mm·year<sup>-1</sup>, respectively, calculated over the period 1942-2017. The Morton equation (Donohue et al., 2010), and the Budyko-curve (Donohue et al., 2007) thus classify the area as dominated by ET, or water-limited (Jackson et al., 2009; Benyon et al., 2006).

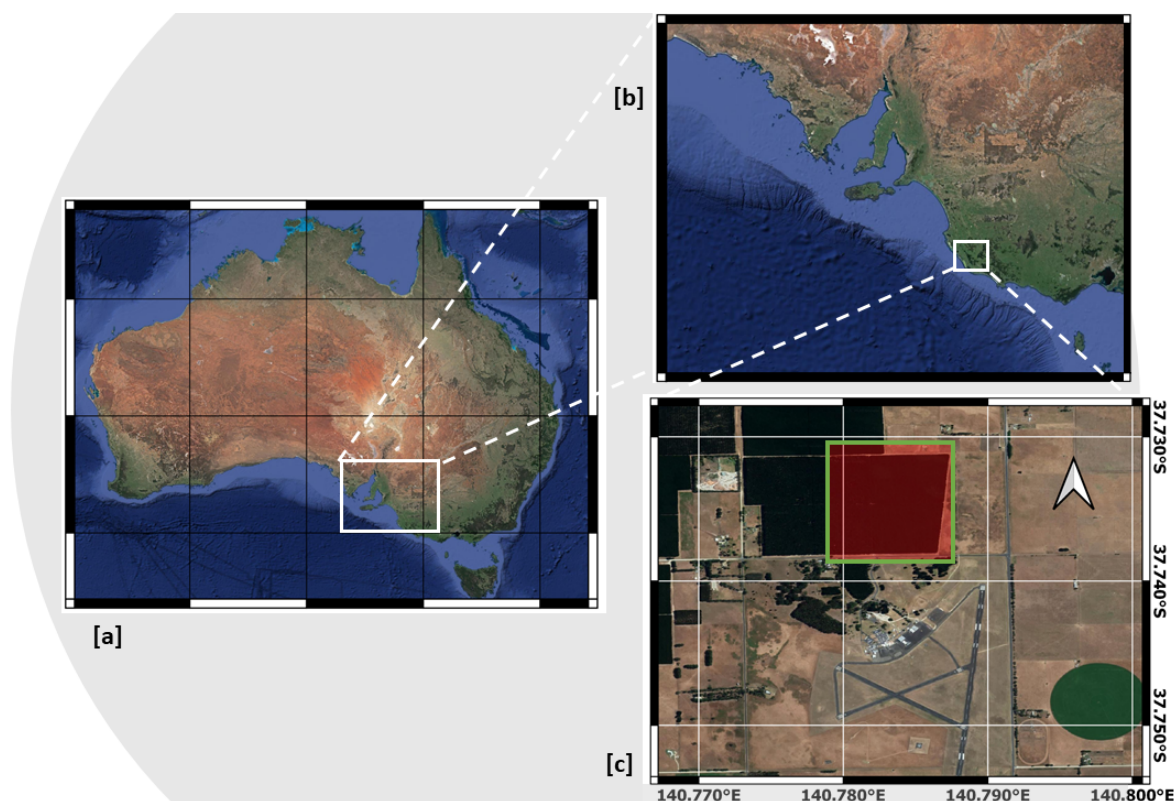


**Figure 1.** Localization of the study area within Australia [a], South East of South Australia [b], detail of the forest plantation [c]. The red square indicates the CMRSET tile. © Google Maps

The study site is a *Pinus Radiata* plantation next to the Mount Gambier airport (Figure 1[c]). The area was originally planted in July 1996 with a density of 1225 trees/ha, there was no thinning of the plantation during the observations. The survey performed by Benyon et al. (2006) classified the soil as duplex. This type of soil presents a contrast between the upper part, which



features sandy-loam characteristics with high hydraulic conductivity, and the lower part, classified as clay, with a finer texture and lower hydraulic conductivity. The average WT depth, from the observations at one bore, is reported at approximately 6 meters below the surface. SM observations were taken at an interval of 30 cm up to 3 meters with a neutron probe. The campaign was conducted from August 2000 to January 2005 with an average measurement frequency of 4 weeks. Because in the area more than 90% of the available groundwater is in shallow aquifers, these plantations have been shown to have direct access to groundwater (Benyon and Doody, 2004).

Remotely sensed data of actual ET from the CSIRO MODIS reflectance-based scaling evapotranspiration (CMRSET) algorithm (Guerschman et al., 2009) were used. These values are obtained by rescaling the PET rates calculated with the Penman-Monteith algorithm using the Enhanced Vegetation Index and Global Vegetation Moisture Index obtained from the MODIS spectroradiometer (Swaffer et al., 2020). The observations are available every 8 days with a finest spatial resolution of 250 by 250 m.

## 2.2 Model Description

Two different configurations of coupled groundwater-unsaturated zone models were tested. The UZMs conceptualization and the coupling to the groundwater model are depicted in Figure 2. This section introduces the models and the coupling framework.

### 2.2.1 UnSAT - UZM

The UnSAT (Unsat<sub>urated</sub> zone & SAT<sub>ellite</sub>) UZM (See Gelsinari et al. (2020) for a detailed description) is a one-dimensional soil water balance model. The unsaturated zone is divided into layers and the water balance of each layer is solved at every time step. The model uses climate forcing data (i.e. precipitation and PET) on a raster distributed basis as inputs, and returns values of actual ET, runoff, recharge and soil water content ( $\theta$ ). The soil is parameterized using the porosity ( $\theta_s$ ), a critical soil-water content to define water stress ( $\theta_*$ ), residual soil-water content ( $\theta_r$ ) (as in Laio et al. (2001)), hydraulic conductivity ( $K_s$ ), and an empirical value for drainage ( $b$ ); the root system is defined using root length ( $l_r$ ) and the root density distribution parameter ( $V_r$ ) as explained in Vrugt et al. (2001). For numerical stability and accuracy the model time step is set to 1 hour.

### 2.2.2 SWAP - UZM

The Soil Water Atmosphere Plant (SWAP v. 4.0) model, developed by Alterra is one of the most used physically-based UZMs (van Dam et al. (2008); Kroes et al. (2017)). This agro-hydrological model applies the Richards equation and is able to simulate the water, heat and solute flow in heterogeneous, variably saturated soils. In addition, it has the potential of accounting for a detailed soil water vegetation interaction as it specifically simulates the dynamics of the crop growth cycle.

125

SWAP has a long history of applications for climate change studies (Droogers et al., 2008; Farkas et al., 2014), fire hazard evaluation (Taufik et al., 2019), impact of land-use change studies (Bennett et al., 2013), water use management (Droogers

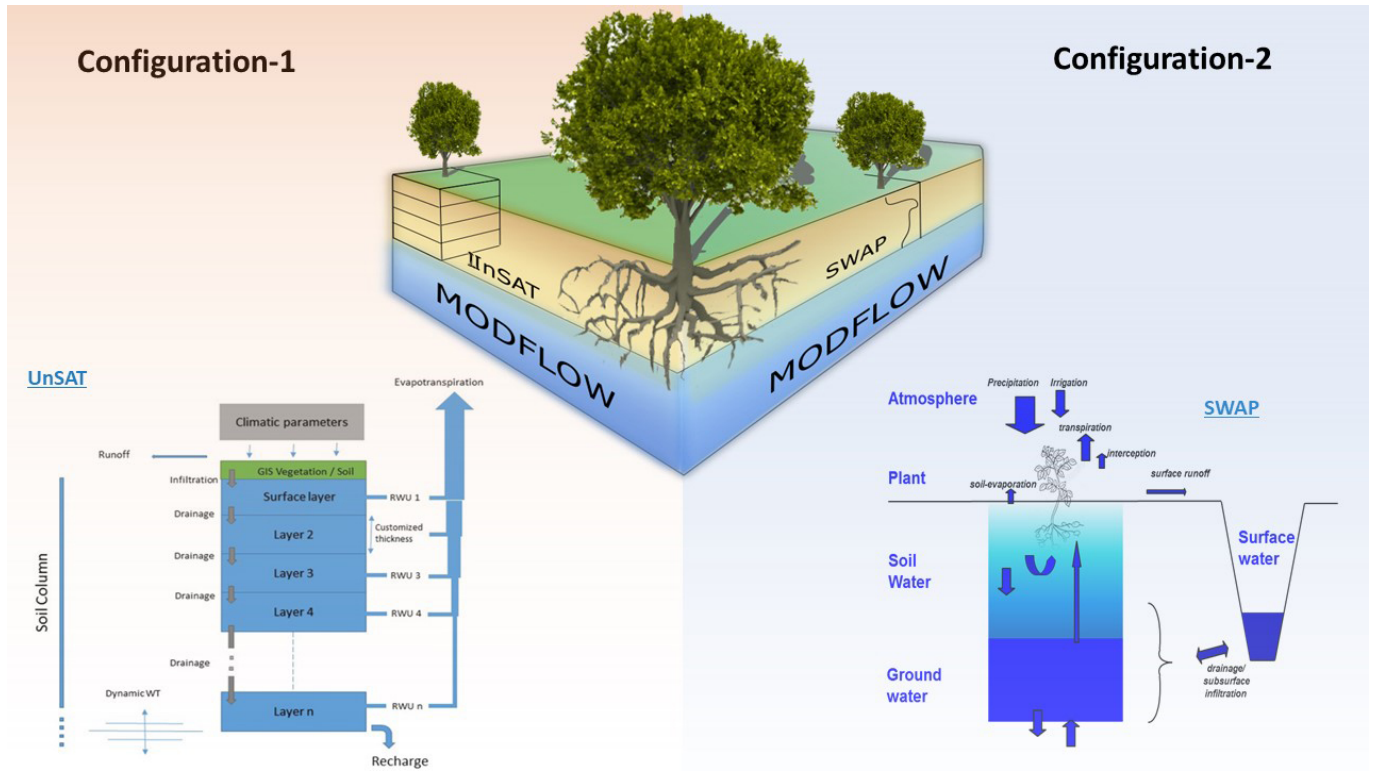


**Figure 2.** Coupled models representation. Left: UnSAT conceptualization coupled to MODFLOW. Right: SWAP conceptualization coupled to MODFLOW.

et al., 2000), groundwater exploitation (Li and Ren, 2019), and holistic assessment of the soil hydraulic properties (Pinheiro et al., 2019).

130

In SWAP, the Richards equation is solved for the pressure head using finite differences. The soil hydraulic retention functions are based on the analytical formulations proposed by van Genuchten (1980). The model requires the van Genuchten soil parameters and a number of vegetation specific parameters (Feddes et al., 1976). In this study, the drought stress parameters are a result of the calibration. These are the pressure head below which water uptake reduction starts (i.e.  $-3000$  mm) and the pressure head triggering no further water extraction (i.e.  $-30000$  mm). The standard root density distribution for forests is used. SWAP has the ability to represent an internal saturated part of the soil column that is controlled by a specified head (simulating drains in the original conceptualization) at the boundary of the domain. In this study, the internal SWAP saturated function is neglected and replaced by the MODFLOW model.

135



### 140 2.2.3 Groundwater Model

The groundwater model chosen for the study is MODFLOW 2005 (Harbaugh, 2005). This modular flexible model has packages dedicated to the calculation of ET and the application of recharge to the groundwater. In this study, the ET package of MODFLOW (EVT) was replaced with the UZMs (UnSAT and SWAP), and the recharge (RCH) package was used to apply the UZMs calculated net-recharge to the cell-specific head.

145

The aquifer saturated hydraulic conductivity ( $K_h$ ) and specific yield ( $S_y$ ) as well as model discretization are defined through FloPy (Bakker et al., 2016), a library that allows MODFLOW to run in a Python environment. The model runs at an 8 day-time step, which is considered adequate for GW dynamics. This choice was made to synchronize the models and assimilation time frequencies as the CMRSET data are available with a temporal resolution of 8 days.

### 150 2.2.4 Coupling

The UZMs were coupled to MODFLOW according to their time steps. UZMs require a shorter time step as the water content varies at a higher frequency than the depth to the WT in the groundwater model (Xu et al., 2012). Variation of the WT at regional scales usually is only appreciable after a period of months or years. Thus, applying a larger time step for the saturated zone model is a valuable option to reduce the computational time (Facchi et al., 2004). At large spatial scales, dimensional  
155 simplification to 1D unsaturated zone flow simulations has been shown to be sound because the direction of the unsaturated zone flow is predominantly vertical (Zhu et al., 2011).

Configuration-1 (Figure 2 left side) features the UnSAT model coupled to MODFLOW through recharge. This configuration specifically accounts for plant transpiration from the WT by calculating the balance between recharge entering the WT  
160 (positive) and transpiration (negative). UnSAT runs at an hourly time step while MODFLOW runs with an 8-day time step, matching the MODIS time step. Once MODFLOW has performed the calculation of the WT levels, these are fed back on a raster basis to UnSAT, which uses them to recalculate the number of layers in which the unsaturated zone is discretized. This dynamic scheme, defined in Zeng et al. (2019) as the non-iterative feedback coupling method, is considered a valuable trade-off between the computational cost of fully coupled or iterative schemes and numerical accuracy.

165

For Configuration-2 (Figure 2 right side) the unsaturated zone is simulated through the SWAP model, with the pressure head along the soil column as state variable. The model has been coupled to MODFLOW through the recharge, similar to the coupling methodology reported by Xu et al. (2012). This way of coupling the model requires caution in the definition of the  $S_y$  parameter, which becomes part of the deterministic calibration and is further explained in section 2.3.

170

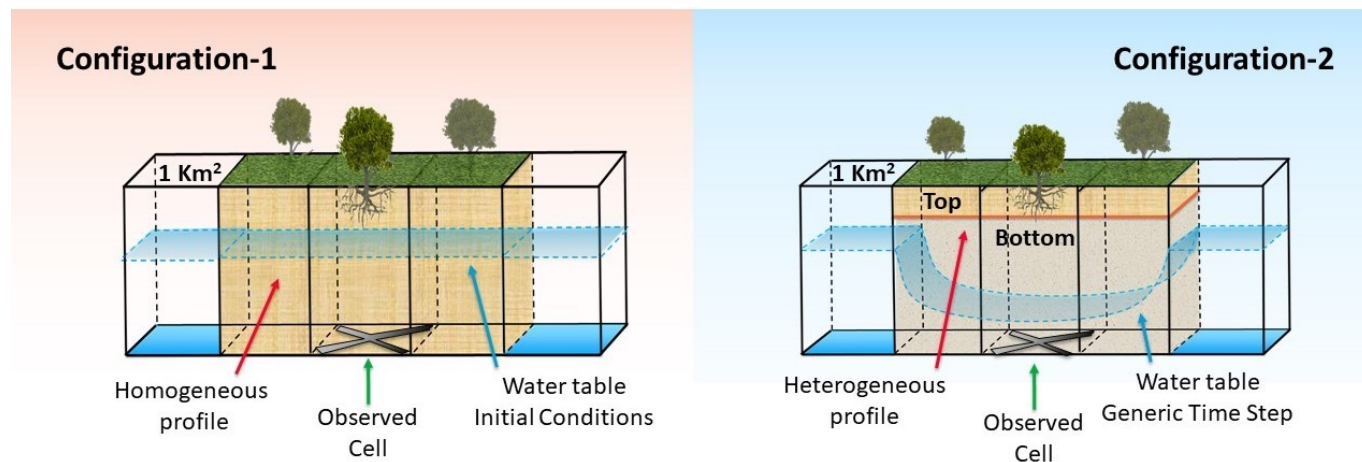


**Figure 3.** Schematic of the simulation domain. Configuration-1 models the unsaturated zone as a homogeneous profile with UnSAT. Configuration-2 models the soil heterogeneity by accounting for the change in soil properties with SWAP. The WT is represented at initial conditions on the left-hand side, and at a generic simulation time, showing the depression caused by the root water extraction, on the right-hand side.

### 2.3 Model Domain and Calibration

The coupled model configurations were applied to a domain of 1 x 5 cells of 1 km<sup>2</sup> each, and a single vertical unconfined layer (Figure 3). The boundary cells were set to a constant head obtained via calibration (See Section 3.1). UnSAT can account for the decrease of  $K_s$  along the soil column, whereas SWAP is capable of explicitly modeling the heterogeneity of the soil column, as described in Section 2.1. Thus, For Configuration-1, the decay of  $K_s$  is a result of the calibration, while other soil parameters are homogeneous along the soil column length (i.e. 10 m). In Configuration-2, the first (Upper) 1.5 meters of soil is classified as "Sandy-Loam" soil and the second (Lower) is a "Loam-Clay" soil spanning the rest of the simulated soil column (i.e. 8.5 m).

180 Preliminary analyses of this study (not shown) indicated that, in order to get significant improvements in the model outputs, the link between WT depth and ET had to be accurately reproduced. For both configurations, attempting to assimilate ET fluxes, without reproducing the interdependence between WT and actual ET, yielded poor filter performances. To account for this interdependence, and reduce the order of freedom of the ill-posed problem of calibration, a multi-objective function (MOF) which combines WT depths and actual ET values was introduced. Then, SM observations were used for refinement and to set  
185 boundaries to the soil parameters. The algorithm Particle Swarm Optimization (PSO) (Kennedy and Eberhart, 1995; Shi and Eberhart, 1998) was used for calibration minimizing the specifically defined MOF:





**Table 1.** Calibrated parameter values used for the simulations and their perturbation fraction.

Model Parameter	Configuration 1	Configuration 2	Perturbation Fraction %
	UnSAT + MODFLOW	SWAP + MODFLOW	
	Homogeneous	Top   Bottom	
Hydraulic conductivity - $K_s$ [ $\text{mm}\cdot\text{hr}^{-1}$ ]	25	24   41	10
Drought Stress (Reduction) [mm]	-	-3000	-
Drought Stress (No extraction) [mm]	-	-30000	-
Oxygen Stress (Reduction) [mm]	-	-100	-
Oxygen Stress (No extraction) [mm]	-	+ 5	-
Soil porosity [ $\text{mm}^3\cdot\text{mm}^{-3}$ ]	0.35	0.36   0.36	-
Critical transpiration $SM(\theta_*)$ [ $\text{mm}^3\cdot\text{mm}^{-3}$ ]	0.12	-	-
Residual $SM(\theta_r)$ [ $\text{mm}^3\cdot\text{mm}^{-3}$ ]	0.03	0.01   0.02	-
Drainage empirical value [-]	2.50	-	-
Root depth [mm]	8000	2900	10
Root distribution parameter ( $V_r$ ) [-]	0.5	-	-
MODFLOW $K_h$ [ $\text{m}\cdot\text{d}^{-1}$ ]	10.0	8.0	10
MODFLOW $S_y$ [-]	0.12	0.11	10

$$\text{MOF} = \frac{\text{RMSE}(WT)}{\sigma(WT)} + \frac{\text{RMSE}(ET)}{\sigma(ET)}, \quad (1)$$

190 where RMSE is the Root Mean Square Error, and  $\sigma$  is standard deviation. PSO searches the n-dimensional solution space, where n is the number of parameters given, in order to minimize equation 1. The calibrated parameters are listed in Table 1. The drainage empirical value and root distribution parameter apply only to Configuration-1. The oxygen stress values, one of which indicates the upper pressure head limit for no extraction and the other the start of the plant transpiration reduction, apply to Configuration-2. The other values are for both configurations.

195

For each configuration, the observation data set was divided into two periods used for calibration and validation. For calibration, 46 8-day time steps covering roughly the year 2001 were used, while the rest of the data set (4.5 years in total) was used for validation.

## 2.4 Assimilation

200 The EnKF (Evensen, 1994) was used because of its ability to deal with highly non-linear systems. The filter initially requires the establishment of a number of ensemble members, generated by perturbing the forcing inputs of precipitation and PET. The



ensemble population size was set to 32, a size which has been widely used for a number of EnKF applications (Mitchell et al., 2002; Pauwels et al., 2013). To verify the spread and accuracy of the ensemble, a number of statistical variables, originally developed for numerical weather prediction by Talagrand et al. (1997), were calculated on the ensemble population.

205

Usually, in data assimilation studies, the assimilated observations are model states, also called prognostic variables, such as SM, pressure head and WT levels. This paper uses actual ET flux observations, which are diagnostic variables of the coupled configurations. Therefore, the interaction between actual ET and model states occurs in the UZM, of which actual ET is a model result. Following the findings of Gelsinari et al. (2020), actual ET data from MODIS (CMRSET data set) are assimilated into the coupled model configurations.

210

The two configurations apply a similar scheme of the EnKF, the difference lying in the composition of the state vector, as the state variables of the UZMs are different. More specifically, the state vector of Configuration-1, for a single ensemble member ( $i = 1, \dots, M$ ) is composed of the WT level  $h$  and the SM values at time step  $s$ , reading

$$215 \quad \mathbf{z}_{[1]k}^{i,f} = [\theta_1 \quad \theta_2 \cdots \theta_n] \cdots, \quad (2)$$

where  $\theta_1, \theta_2, \dots, \theta_n$  are the SM values of the UZM layers, for the  $i$ -th ensemble member, and  $f$  means forecast.

For Configuration-2, the state vector is similarly composed and reads

$$\mathbf{z}_{[2]k}^{i,f} = [p_1 \quad p_2 \cdots p_n] \quad (3)$$

220 where, for the  $i$ -th ensemble member,  $p_1, p_2, \dots, p_n$  are the pressure head values for each layer of the UZM. The filter scheme is then similarly applied for both configurations as follows.

The aggregated state vector for the assimilation time step  $k$  and the ensemble member  $i$  is then composed in the same fashion for both configurations. The aggregated vector of Configuration-1 is

$$\mathbf{x}_k^{i,f} = [h^{i,f}, \quad \mathbf{z}_{[1]1}^{i,f}, \mathbf{z}_{[1]2}^{i,f}, \dots, \mathbf{z}_{[1]t}^{i,f}]^T, \quad (4)$$

225 where  $t$  is the number of times the UZM model is applied during the assimilation time step, which is different in the two configurations, T indicates the transposed vector, and  $h$  is the WT level, permanent during the  $t$  time steps, simulated by MODFLOW.

The observation from the CMRSET for the  $k$  time step is the vector

$$\mathbf{y}_k = [ET_k]. \quad (5)$$



230 The remainder of the assimilation algorithm is described in Gelsinari et al. (2020). According to their findings, the state variable update had to be limited to preserve numerical stability. This was equally true for both models and applies specifically to the WT levels. A limitation of  $\pm 50\%$  of the prior values is applied for the SM content of Configuration-1 and, similarly, to the pressure head variable of Configuration-2. This avoids the convergence problem in physically based models reported in Zhang et al. (2018).

#### 235 2.4.1 Ensemble Generation

The generation of a statistically meaningful ensemble, which preserves the relationship between ET and WT levels obtained during the calibration, is crucial for the application of the EnKF (Gelsinari et al., 2020). A number of ensemble generation techniques were applied to the two configurations, and a consistent approach for both configurations was adopted. First, a simple perturbation of forcing inputs, by adding a random number sampled from Gaussian distributions with different standard deviations, as performed by Gelsinari et al. (2020), was tested. Then, a mixed method involving the perturbation of both inputs and the parameters, with the latter perturbed by adding a random number proportionally to the calibrated value, was applied. For the UZMs, the parameters selected for the perturbation were  $K_s$  and root depth, and for MODFLOW the saturated  $K_h$  and  $S_y$ . Initial conditions of WT levels were also perturbed to induce a good spread in the ensemble from the early stages of the simulation. This ensemble of simulations is defined as the open loop, which represents the "prior" distribution. After applying the filter, the resulting distribution is called the assimilation run and represents the "posterior".

In such a nonlinear configuration, it is a challenge to generate ensembles that maintain the statistical accuracy, and simultaneously preserve the ET - WT relationship. The most adequate ensembles for the two configurations, obtained by calculating the ensemble validation skills on the modeled ET based on the method explained in Talagrand et al. (1997), were retained (De Lannoy et al., 2006; Pauwels and De Lannoy, 2009). Results are shown in Section 3.2).

#### 2.5 Verification skills

The assimilation skills are evaluated using the Root Mean Square Error (RMSE) and the Pearson correlation coefficient ( $r$ ) defined as:

$$\text{RMSE} = \sqrt{\frac{1}{L} \sum_{k=1}^L (o_k - f_k)^2}, \quad (6)$$

$$r = \frac{\sum_{k=1}^L (o_k - \bar{o})(f_k - \bar{f})}{\sqrt{\sum_{k=1}^L (o_k - \bar{o})^2 \cdot \sum_{k=1}^L (f_k - \bar{f})^2}}. \quad (7)$$



**Table 2.** Results for the calibrated runs.

Variable	Configuration	RMSE	$r$
WT Levels	1	0.230 [m]	0.790
	2	0.360 [m]	0.400
SM Upper	1	0.049 [mm <sup>3</sup> mm <sup>-3</sup> ]	0.410
	2	0.045 [mm <sup>3</sup> mm <sup>-3</sup> ]	0.610
SM Lower	1	0.085 [mm <sup>3</sup> mm <sup>-3</sup> ]	0.592
	2	0.018 [mm <sup>3</sup> mm <sup>-3</sup> ]	0.850
ET	1	0.791 [mm day <sup>-1</sup> ]	0.811
	2	0.870 [mm day <sup>-1</sup> ]	0.788

Here,  $o_k$  is the observation and  $f_k$  is the modeled variable at time  $k$  and  $L$  is the size of the data set. The filter performance are assessed comparing these metrics, applied to the assimilation results, to the respective open loop run.

### 3 Results and Discussion

#### 3.1 Deterministic Runs

260 During the calibration with the PSO, the dynamics of the parameter optimization algorithm was monitored, showing that the MODFLOW saturated hydraulic conductivity ( $K_h$ ) had a consistent tendency towards high values (100 m·d<sup>-1</sup> or higher) in order to minimize Equation 1. This was interpreted as an effect of ET component on the objective function ET component, which was inducing the UZMs to transpire water directly from the WT to compensate for the low ET values. The boundary conditions for the groundwater model were thus modified by imposing a constant head boundary with shallower WT depth,  
265 which maintained  $K_h$  at a plausible order of magnitude. Conceptually, these boundary conditions represent the water supplied from the regional aquifer to the plantation, and induce the WT depression shown on the right hand side of Figure 3.

The calibration technique proposed in Section 2.3 was able to reproduce the link between the WT dynamics and ET for both configurations (See figure 4). Configuration-1 performs better overall in the representation of the WT dynamics with a  
270 RMSE of 0.23 m, while the RMSE of Configuration-2 is slightly larger (i.e. 0.36 m). Configuration-1 also shows a higher correlation coefficient (0.790 vs 0.400) for the WT. Configuration-1 shows a lower temporal variability than Configuration-2, but the latter better matches the temporal evolution of the WT. There is a time lag between groundwater observations and model WT fluctuation for Configuration-2, which also explains the higher RMSE and lower correlation. This lag may be induced by preferential flow that the Richards equation does not account for, or to a slower response of the WT to the meteorological input  
275 that is discussed later in this section.

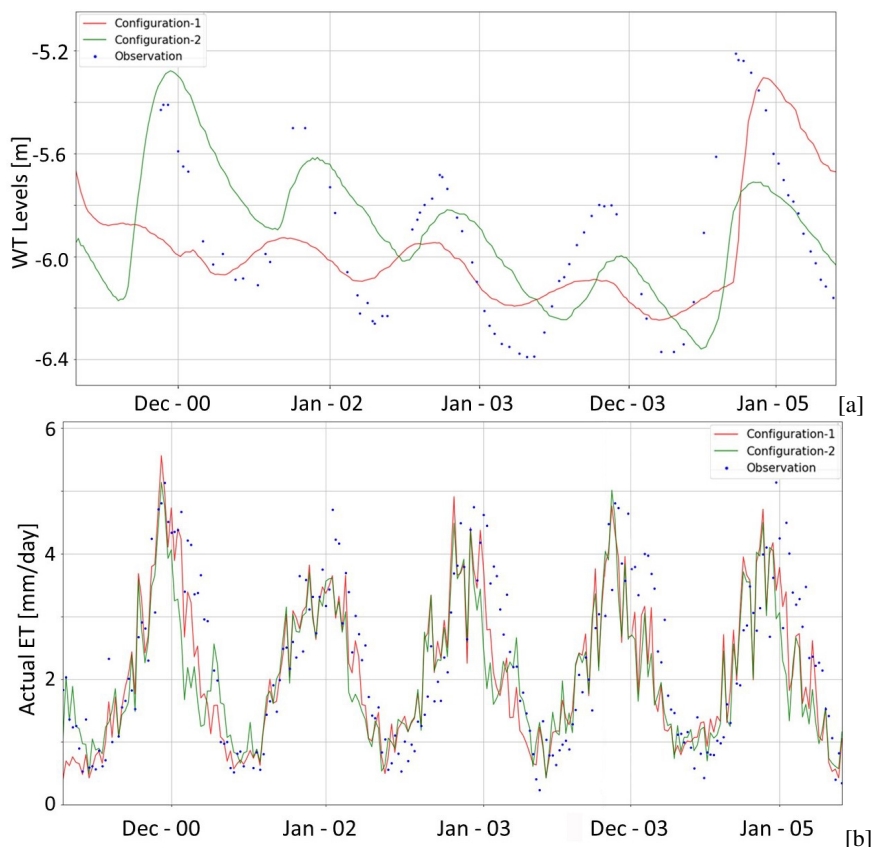


**Figure 4.** Combined WT fluctuations for the two configurations plotted over the observed WT levels [a]. Modeled actual ET [b] for both configurations plotted over the remotely sensed actual ET observations.

The capillary fringe and soil heterogeneity are represented differently by the two configurations. For physically-based Configuration-2, the detail of the capillary fringe is represented in Figure 5 [d] by the blurred area above the saturated zone (i.e. dark blue). Configuration-2 is also able to represent the heterogeneity of the soil column, as shown in Figure 5 [d] where a sharp variation of the SM content at 1.5 m depth is caused by the different soil parameters. Configuration-1 has no ability to represent the capillary fringe effect, and it does not explicitly account for duplex soil. However, it can account for a decay of the hydraulic conductivity along the soil column. Because of these reasons, the modeled SM from Configuration-2 shows a good agreement with the observations, especially in the lower soil (Figure 5 [f]). Configuration-1 has a low SM RMSE ( $0.049 \text{ mm}^3 \cdot \text{mm}^{-3}$ ) and a reasonable agreement in terms of the Pearson correlation coefficient  $r$  (0.410) for the upper soil [b], but the resulting SM is consistently below the observed values in the bottom soil (panel [c]), with an RMSE of  $0.137 \text{ mm}^3 \cdot \text{mm}^{-3}$ . Both configurations report a higher correlation for the lower soil.

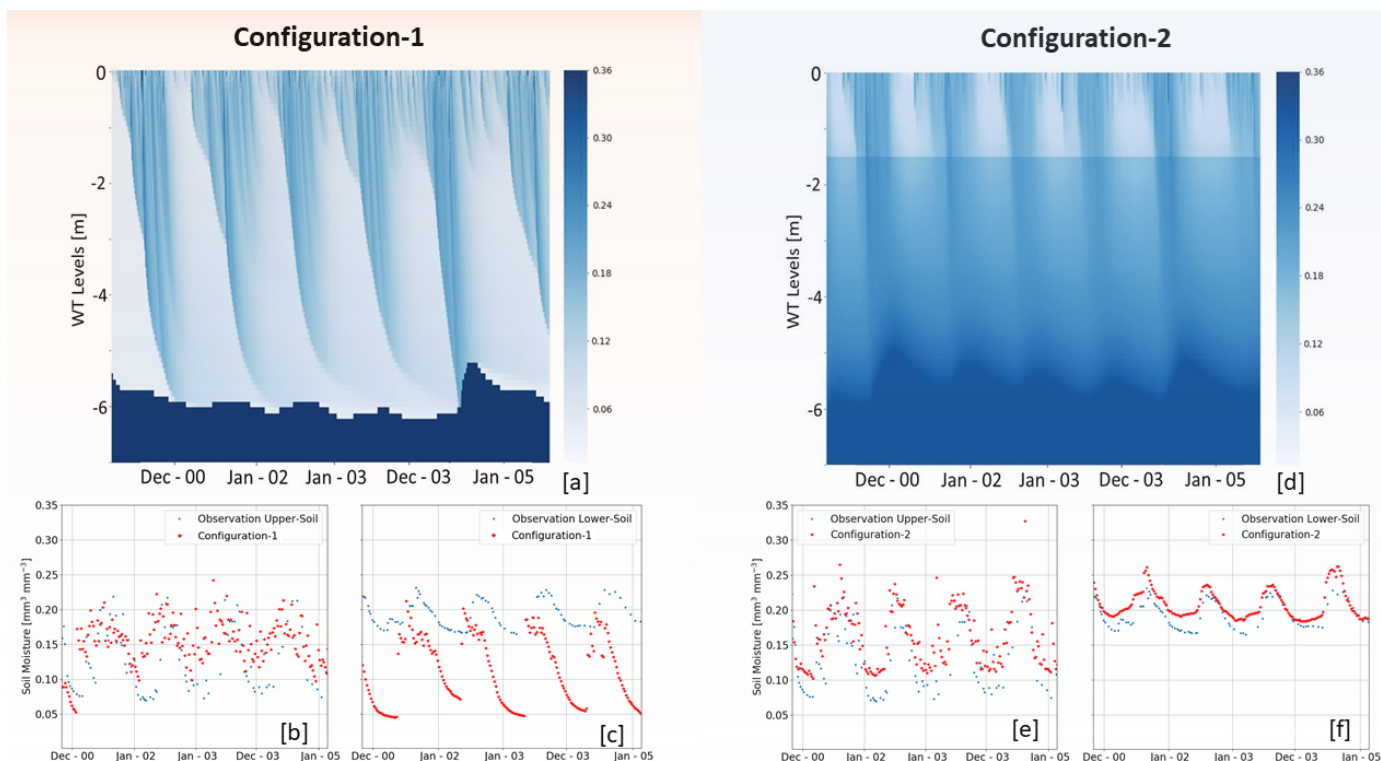


**Figure 5.** Temporal evolution of the SM contents. Panels [a] and [d] show the entire modeled column, including the fluctuation of the WT (i.e. the dark blue area). Panel [b] and [e] represent the modeled and observed water content for the upper soil (averaged over 0-300 mm depth). Panel [c] and [f] show these results for the lower soil (averaged over the interval 1500-1800 mm depth).

For ET, Configuration-1 yields good results with a lower RMSE and similar correlation when compared to Configuration-2. In particular, the physically-based Configuration-2, underestimates the simulated ET for the Southern hemisphere late summer/early autumn as shown in Figure 4 [b]. In this period, the soil water content is low, as shown in Figure 5 [d], and the system is actively transpiring from the groundwater. This can be interpreted as an effect of the coupling to the groundwater model. The conceptually based Configuration-1, with a rooting depth of 8.0 m, is able to extract water directly from the water table and immediately transforms it into ET. Configuration-2, with a rooting depth of 2.9 m, achieves this by reducing the pressure head along the soil column. Thus water has to flow across a part of unsaturated zone before becoming available for direct plant transpiration, reducing the rapid response of the model to the forcing inputs. This also explains the lag in the WT dynamics previously described. Another possible reason for the underestimation of ET are the two oxygen stress parameters that reduce transpiration in conditions close to saturation (Table 1). These parameters are calibrated and kept constant during the simulation period. Configuration-2 has shown to be highly sensitive to these parameters, while Configuration-1 does not



include this process.

300

### 3.2 Ensemble simulations

The generation of the ensemble is also found to be a key step of the method. The simple perturbation of forcing inputs was not able to generate a sufficiently broad ensemble spread, particularly for Configuration-2. For both configurations, the combined perturbation of parameters and forcing inputs was found to produce adequate ensembles. This is obtained by applying the ensemble validation, as discussed in Section 2.4.1, to the first year of the data set, excluding the first 10 time steps to avoid the influence of the initial conditions (i.e. from the 10 to the 45th time step). For the meteorological data, the best candidates are obtained by perturbing the input with a random number sampled from a Gaussian distribution having a standard deviation proportional to the value of the forcing inputs (i.e. 50% for Configuration-1 and 10% for Configuration-2). For the parameters, last column of Table 1 lists the perturbation fractions. Additionally, for Configuration-2,  $S_y$  has a lower limit of 0.1 to preserve numerical stability of the coupled models.

305

310

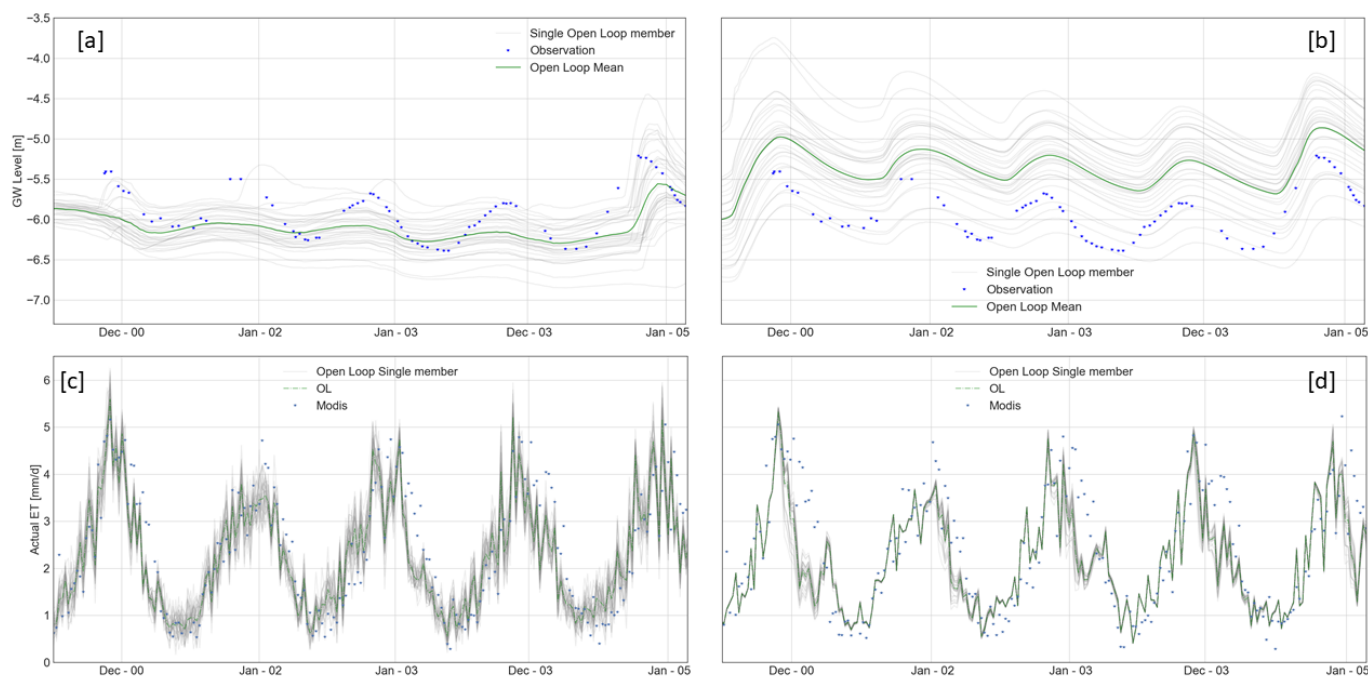


**Figure 6.** WT levels and actual ET and spread of the open loop ensembles for Configuration-1 [a,c] and Configuration-2[b,d]

In the case of the conceptual Configuration-1, the WT level spread of the open loop ensemble is consistently covering the observations (Figure 6[a]). The mean of the ensemble is close to the observations, but does not follow the seasonal variability appropriately. The associated spread of the actual ET for Configuration-1 is wider than that of Configuration-2. More specif-



315 ically, the latter is narrow during wet periods (i.e. April to November) and becomes wider for the dry period (Figures 6[c]  
 and 6[d]). A similar effect, with a larger magnitude, was reported during the ensemble generation phase and led to the double  
 perturbation of the meteorological inputs and the parameters as explained in Section 2.4.1.

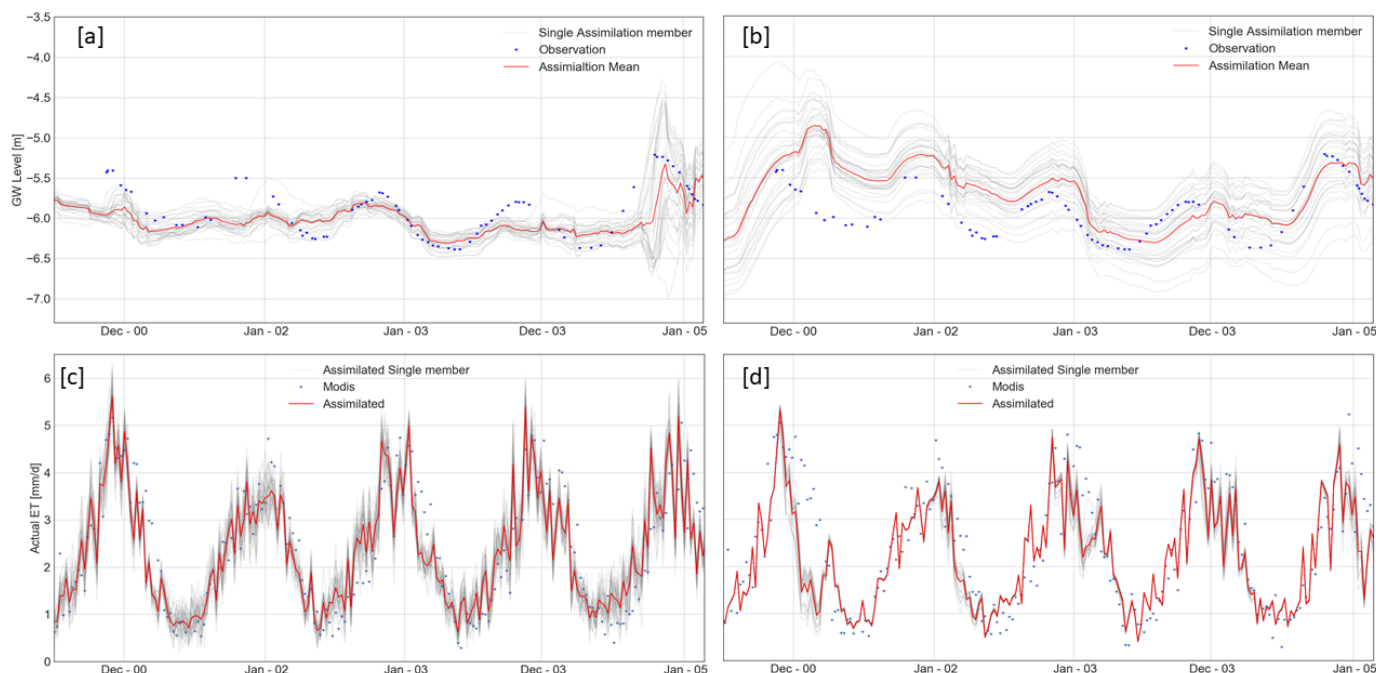


**Figure 7.** WT levels and actual ET and spread of the assimilation run for Configuration-1 [a,c] and Configuration-2 [b,d]

The spread of the WT levels for Configuration-2 (see panel [b]) covers the WT observations for most of the simulations  
 and is wider than for Configuration-1. The mean represents the amplitude of the seasonal fluctuations better as compared to  
 320 Configuration-1, but leads to a shallower WT as a result of the perturbation of the forcing inputs.

**Table 3.** RMSE and correlation for three variables between the open loop and the assimilation.

Config	Type	Actual ET		WT Levels		SM Upper Soil		SM Lower Soil	
		RMSE	<i>r</i>	RMSE	<i>r</i>	RMSE	<i>r</i>	RMSE	<i>r</i>
1	Open loop	0.760	0.820	0.280	0.730	0.045	0.497	0.102	0.468
	Assimilation	0.730	0.830	0.236	0.734	0.044	0.498	0.098	0.428
2	Open loop	0.830	0.810	0.626	0.880	0.041	0.888	0.019	0.940
	Assimilation	0.810	0.820	0.307	0.675	0.042	0.864	0.017	0.900



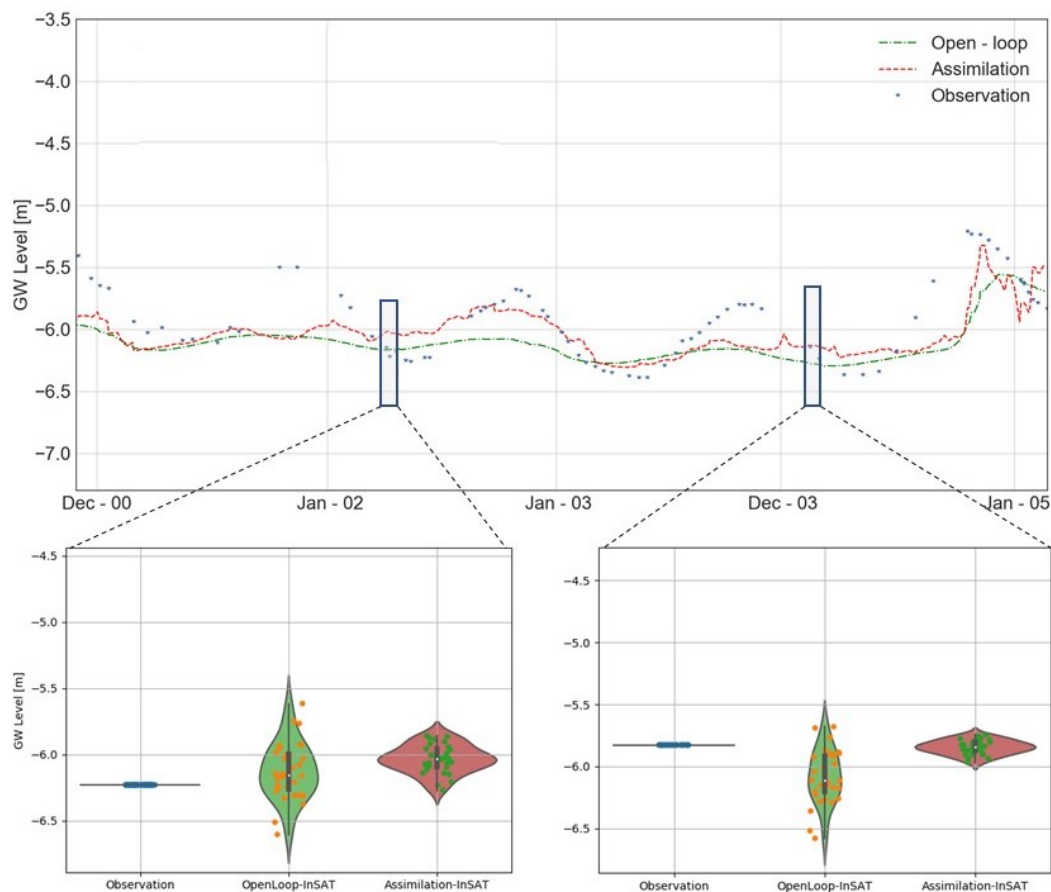


Table 3 summarizes and compares the results between the open loop and the assimilation for actual ET, WT levels, and SM contents of the upper and lower soil layers. For both configurations, the ET assimilation slightly decreases the RMSE and improves the correlations. In particular, the RMSE of ET for Configuration-1 reduces from  $0.76 \text{ mm}\cdot\text{day}^{-1}$  for the open loop  
325 to  $0.73 \text{ mm}\cdot\text{day}^{-1}$ . The RMSE for the ET for Configuration-2 reduces from  $0.83 \text{ mm}\cdot\text{day}^{-1}$  for the open loop to  $0.81 \text{ mm}\cdot\text{day}^{-1}$ . The correlation also improves marginally for both configurations (i.e. + 0.01). However, these are non-trivial results as the data assimilation, through the EnKF, is designed to improve the model states. Therefore, the reduction of the ET errors suggests that the improved state variables are contributing to a better modeling of other hydrological quantities.

330 In Configuration-2, the assimilation is not able to improve ET in the Summer of 2000/2001 and 2002/2003. This results in poorer WT simulations during these periods (Figure 7[b]). Here, the filter is trying to increase the amount of water in the system to match the higher assimilated observation, which is a correct application of the methodology. Thus, the WT is made shallower by the filter but this does not reflect in a higher modeled ET. The reason for this is the behaviour of the SWAP vegetation parameter oxygen stress. The filter is increasing the pressure head of the system, in an attempt to provide more water to  
335 transpire, but the actual transpiration from the plant is hindered by SWAP, which recognizes the soil to be too saturated for the plant to transpire. The EnKF then causes the WT to rise, and increases the amount of recharge entering the groundwater. When the observed ET is lower than the simulations, the filter reduces the pressure head and the model allows the plant to transpire. Therefore, in the two time steps after this effect, the modeled ET is higher than the observation, after which this phenomenon disappears. This artefact is not seen in Configuration-1 as the oxygen stress is not accounted for.

340 Figures 8 and 9 show the observations, the mean of the open loop (blue dash-dotted line) and the mean of the assimilation runs (red dot line), for Configuration-1 and Configuration-2, respectively. For both configurations, the assimilation improves the RMSE when compared to the open loop runs. The best results are obtained for Configuration-1, showing a RMSE of 0.236 m with a 15 % error reduction compared to the open loop. Configuration-2 resulted in a substantial error reduction of 38.9 %  
345 as compared to the open loop. However, the overall RMSE value (0.307 m) is still higher than Configuration-1. Apart from the oxygen stress artefacts explained above, the assimilation run of Configuration-2 is consistently better than the open loop. This is not always the case for Configuration-1, where the open loop was already performing well. The correlation remains largely unchanged for Configuration-1, and reduces for Configuration-2 mainly due to the updates during the summers of 2000/2001 and 2002/2003.

350 The two violin plots shown in the insets to Figure 8 and 9 provide a visual representation of the magnitude of uncertainty before (prior) and after (posterior) the assimilation. In general, the spread of the WT levels for Configuration-1 is narrower than the equivalent for Configuration-2. Even when the mean of the open loop is closer to the observation, as in the first violin plot of figure 8, the assimilation helps in reducing the uncertainty around the WT levels. The second violin plot shows an  
355 ideal situation, where the assimilation mean is very close to the observed value and the uncertainty interval is narrow. This combination was not obtained for Configuration-2. As shown in the violin plots of figure 9, the posterior covariances (i.e. the



**Figure 8.** Observations, open loop mean and assimilation mean for Configuration-1. In the insets the green and red surfaces represent the violin plots of the open loop (Prior) and the assimilation runs (Posterior) distributions, respectively, for two dates indicated by the boxes.

red violin plot) are still large after the assimilation. This means a lower uncertainty reduction compared to Configuration-1.

Figure 10 presents the scatter plots of the SM in the top (at a depth of 300 mm) and bottom (1800 mm) parts of the soil  
 360 for each configuration. The open loop of Configuration-1 has an RMSE of  $0.045 \text{ mm}^3 \cdot \text{mm}^{-3}$  for the upper soil and  $0.102 \text{ mm}^3 \cdot \text{mm}^{-3}$  for the lower soil. In the latter, the simulated water contents are consistently lower than the observations. This is mainly due to the model's inability to represent capillary rise. The assimilation only marginally improved the SM content, with slightly better results for the bottom part of the soil, where the RMSE was reduced to  $0.098 \text{ mm}^3 \cdot \text{mm}^{-3}$ . The open loop of Configuration-2 has a lower RMSE,  $0.041$  and  $0.017 \text{ mm}^3 \cdot \text{mm}^{-3}$  for the top and bottom part of the soil, respectively. However,  
 365 it is slightly overestimating the SM content for the entire column. This is consistent with the shallower WT (i.e. more water in the system) observed for the WT levels in the open loop (Figure 6[d]). The assimilation did not improve the top layer SM content, with an RMSE of  $0.042 \text{ mm}^3 \cdot \text{mm}^{-3}$ . However, the assimilation improved the SM content of the bottom part (Figures

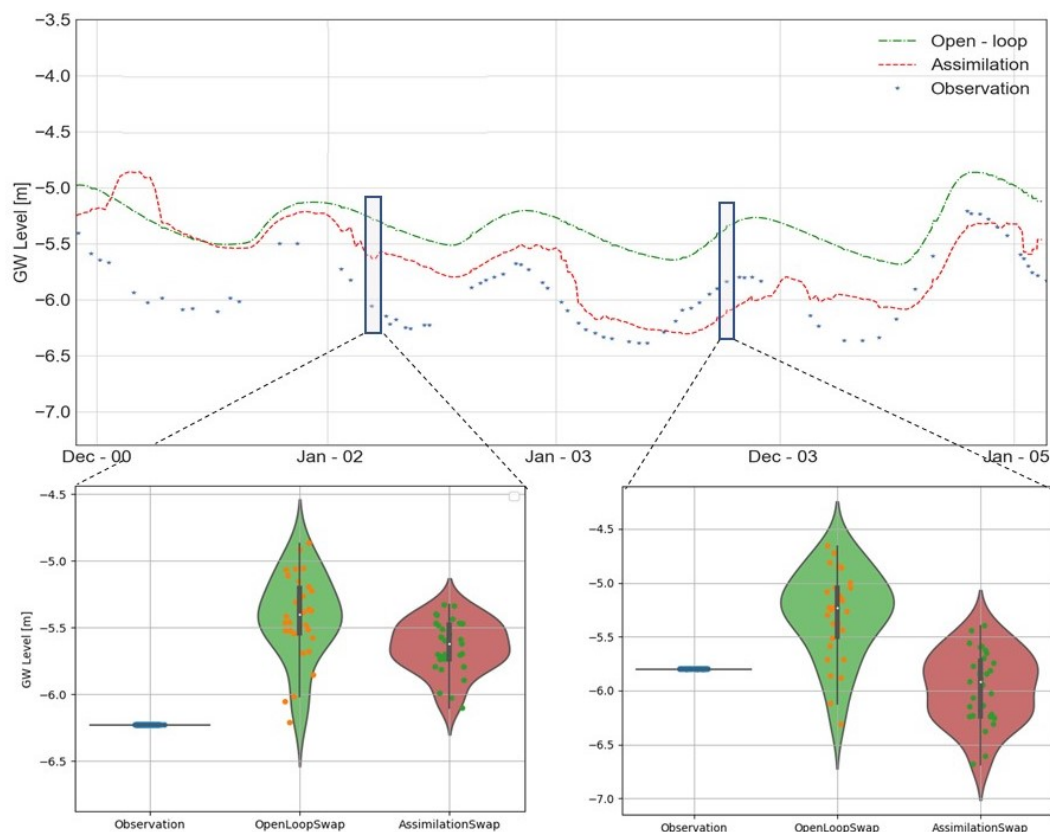


**Figure 9.** Observations, open loop mean and assimilation mean for Configuration-2. In the insets the green and red surfaces represent the violin plots of the open loop (Prior) and the assimilation runs (Posterior) distributions, respectively, for two dates indicated by the boxes.

10[g] and [h]), for which the best results are obtained (i.e. 0.015). The updating of the entire soil column is a positive result of the assimilation of ET rates, as opposed to the assimilation of remotely sensed SM values. The latter usually results in stronger updates in the upper parts of the soil, because of the reduced correlation between the SM contents in the upper and deeper parts of the soil column.

Generally, these results consolidate the synthetic approach in Gelsinari et al. (2020), and further confirm that the assimilation framework is not only able to update and improve the WT level, which is a prognostic variable of the coupled model, but also the modeled ET, and consequently the recharge to the WT. In addition, albeit marginally, the filter improves the unsaturated zone state variables regardless of the manner in which the SM content is calculated (volumetric SM or pressure head).

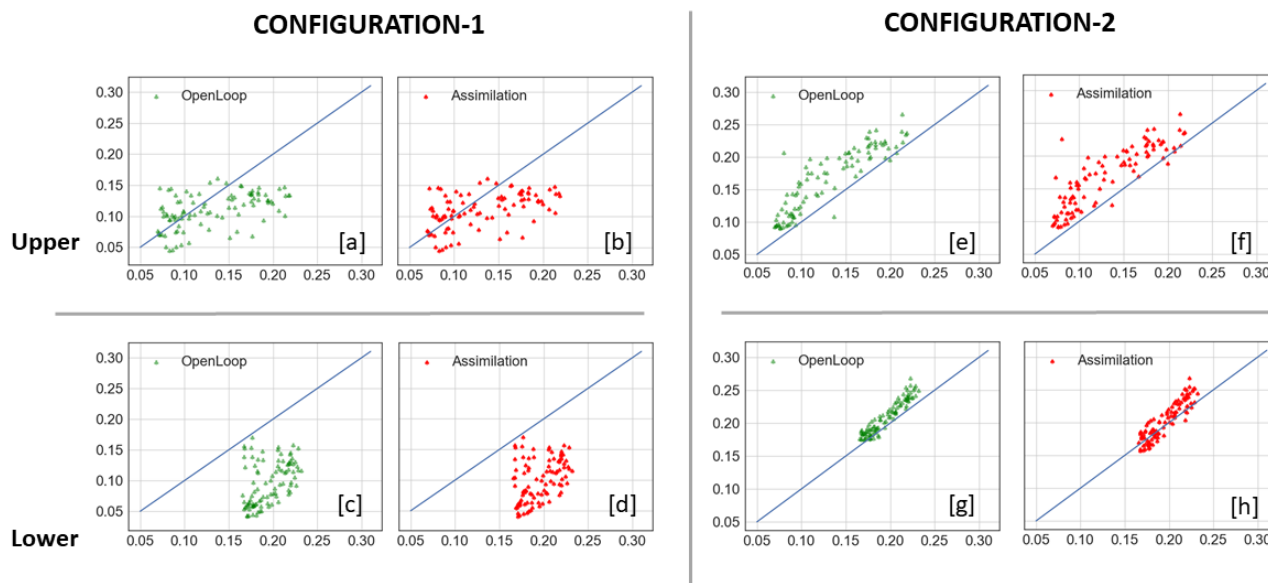


**Figure 10.** Scatter plots of the upper [a,b,e,f] and lower [c,d,g,h] soil water content. Configuration-1 open-loop [a,c], Assimilation [b,d]. Configuration-2 open-loop [e,g], Assimilation [f,h]. N.B. Observations are reported on the x axes.

#### 4 Conclusions

This study validates the assimilation of the satellite-based evapotranspiration (ET) data set (CMRSET) into two coupled unsaturated zone-groundwater configurations. Specifically, these configurations are composed by a conceptual water balance model (UnSAT) and a physically-based agro-hydrological model (SWAP), respectively, coupled to MODFLOW and applied to a semi-arid, pine plantation in the south-east of South Australia.

The most important findings can be summarized as:

**Calibration.** This study shows the need to calibrate the model using a multi-objective function, with normalised components of water table (WT) and actual ET. In this way, both configurations are representing the WT-ET relationship in an appropriate manner and benefit from the assimilation of ET observations.

**Configuration-1.** The assimilation of ET values through the Ensemble Kalman Filter (EnKF) using a conceptual unsaturated zone model, produced the best results for the prognostic variable WT levels and the diagnostic fluxes of actual ET. SM values were also slightly improved in both the upper and lower parts of the soil column. However, because of the model conceptualization the mismatch in the lower part of the soil is considerably larger than for Configuration-2. The reduced number of parameters of this configuration allows for a simpler calibration, which is able to represent the



WT dynamics. Similarly, the generation of an appropriate ensemble is more straightforward mostly due to the model conceptualization, which allows the WT to respond quickly to direct root water extraction by transpiration.

**Configuration-2.** The ET assimilation into a physically-based unsaturated zone model, based on the Richards equation, produced the largest improvements to the WT levels with a larger uncertainty reduction and an adequate representation of the capillary fringe. Improvements to actual ET fluxes were similar to Configuration-1. For SM, generally the impact of the assimilation algorithm was small, with a positive update for the lower soil layers, and a negative update for the upper layers. Here, the calibration involved a larger number of parameters and produced a good representation of the SM dynamics. However, due to the non-linearity introduced with the coupling (e.g. capillary fringe), errors in the WT levels and ET fluxes are higher. In addition, the ensemble generation is constrained by the high model parameterization, making it more difficult to produce an appropriate ensemble that preserves the ET-WT relationship.

**ET information.** The updating of the entire soil column is an advantage of the assimilation of remotely sensed ET over satellite SM retrievals. ET rates express the moisture status of the entire root zone. Thus, assimilating ET overcomes the SM assimilation tendency to produce stronger updates in the most superficial part of the soil because of the reduced correlation between the upper and lower SM contents.

In conclusion, it is possible to use either a conceptual or a physically-based unsaturated zone model in the assimilation of satellite-based ET estimates to inform hydrogeological models. Both model coupling configurations reduce the uncertainty related to state variables (such as WT and SM) and fluxes of actual ET. The findings indicate that a simple conceptual model may be sufficient for this purpose, thus using one configuration over the other should be only motivated by the specific purpose of the simulation and the information available. This study represents a step towards the use of satellite-based ET retrievals for water resources management. For future applications at larger scales, more research is to be conducted in areas with different groundwater, vegetation and soil conditions, with the intent of prioritizing regions where the ET assimilation is more effective.

*Data availability.* Forcing input <http://www.bom.gov.au/>

Results: <https://figshare.com/s/222b9874a7ff328a8a24>

(Would become <https://doi.org/10.26180/5ec4cda0b2612> upon publication)

CMRSET: <https://doi.org/10.25919/5c36d76d2ac2f/>

*Author contributions.* SG performed the modelling work and wrote the manuscript. VP supervised the implementation of the EnK, ED supervised the implementation of the UnSAT model, JvD supervised the implementation and coupling of the SWAP model, and RD supervised the entire project. All co-authors also provided input to the writing of the manuscript.



*Competing interests.* No competing interests were found

*Acknowledgements.* Funding for this project has been provided by the CSIRO Land & Water Effective Floodplain Management Project. SG acknowledges the financial support by the Faculty of Engineering at Monash University through the Graduate Research International Travel Award and thanks the chair group of Hydrology and Quantitative Water Management at Wageningen University & Research for the support  
425 during his visit. SG also thanks Karina Gutierrez Jurado for her support and suggestions during the preparation of this manuscript



## References

- Bakker, M., Post, V., Langevin, C. D., Hughes, J. D., White, J. T., Starn, J. J., and Fioren, M. N.: Scripting MODFLOW Model Development Using Python and FloPy, *Groundwater*, 54, 733–739, <https://doi.org/10.1111/gwat.12413>, <http://doi.wiley.com/10.1111/gwat.12413>, 2016.
- 430 Banks, E. W., Brunner, P., and Simmons, C. T.: Vegetation controls on variably saturated processes between surface water and groundwater and their impact on the state of connection, *Water Resour. Res.*, 47, 1–14, <https://doi.org/10.1029/2011WR010544>, 2011.
- Batelaan, O. and De Smedt, F.: GIS-based recharge estimation by coupling surface-subsurface water balances, *J. Hydrol.*, 337, 337–355, <https://doi.org/10.1016/j.jhydrol.2007.02.001>, 2007.
- Bennett, S. J., Bishop, T. F., and Vervoort, R. W.: Using SWAP to quantify space and time related uncertainty in deep drainage model estimates: A case study from northern NSW, Australia, *Agric. Water Manag.*, 130, 142–153, <https://doi.org/10.1016/j.agwat.2013.08.020>, <http://dx.doi.org/10.1016/j.agwat.2013.08.020>, 2013.
- 435 Benyon, R. G. and Doody, T. M.: Water Use by Tree Plantations in South East South Australia. CSIRO Forestry and Forest Products, Tech. rep., CSIRO, <http://www.ffp.csiro.au/http://www.dwlbc.sa.gov.au/http://www.secatchment.com.au/>, 2004.
- Benyon, R. G., Theiveyanathan, S., and Doody, T. M.: Impacts of tree plantations on groundwater in south-eastern Australia, *Aust. J. Bot.*, 54, 181, <https://doi.org/10.1071/BT05046>, <http://www.publish.csiro.au/?paper=BT05046>, 2006.
- 440 Camporese, M., Paniconi, C., Putti, M., and Orlandini, S.: Surface-subsurface flow modeling with path-based runoff routing, boundary condition-based coupling, and assimilation of multisource observation data, *Water Resour. Res.*, 46, <https://doi.org/10.1029/2008WR007536>, 2010.
- Carroll, R. W. H., Pohl, G. M., Morton, C. G., and Huntington, J. L.: Calibrating a Basin-Scale Groundwater Model to Remotely Sensed Estimates of Groundwater Evapotranspiration, *J. Am. Water Resour. Assoc.*, <https://doi.org/10.1111/jawr.12285>, 2015.
- 445 De Lannoy, G. J., Houser, P. R., Pauwels, V. R., and Verhoest, N. E.: Assessment of model uncertainty for soil moisture through ensemble verification, *J. Geophys. Res. Atmos.*, 111, <https://doi.org/10.1029/2005JD006367>, 2006.
- Doble, R. C., Pickett, T., Crosbie, R. S., Morgan, L. K., Turnadge, C., and Davies, P. J.: Emulation of recharge and evapotranspiration processes in shallow groundwater systems, *J. Hydrol.*, 555, 894–908, <https://doi.org/10.1016/j.jhydrol.2017.10.065>, <https://doi.org/10.1016/j.jhydrol.2017.10.065https://linkinghub.elsevier.com/retrieve/pii/S0022169417307424>, 2017.
- 450 Donohue, R. J., Roderick, M. L., and McVicar, T. R.: On the importance of including vegetation dynamics in Budyko’s hydrological model, *Hydrol. Earth Syst. Sci.*, 11, 983–995, <https://doi.org/10.5194/hess-11-983-2007>, 2007.
- Donohue, R. J., McVicar, T. R., and Roderick, M. L.: Assessing the ability of potential evaporation formulations to capture the dynamics in evaporative demand within a changing climate, *J. Hydrol.*, 386, 186–197, <https://doi.org/10.1016/j.jhydrol.2010.03.020>, <http://linkinghub.elsevier.com/retrieve/pii/S0022169410001460>, 2010.
- 455 Droogers, P., Bastiaanssen, W. G., Beyazgül, M., Kayam, Y., Kite, G. W., and Murray-Rust, H.: Distributed agro-hydrological modeling of an irrigation system in western Turkey, *Agric. Water Manag.*, 43, 183–202, [https://doi.org/10.1016/S0378-3774\(99\)00055-4](https://doi.org/10.1016/S0378-3774(99)00055-4), 2000.
- Droogers, P., van Loon, A., and Immerzeel, W. W.: Quantifying the impact of model inaccuracy in climate change impact assessment studies using an agro-hydrological model, *Hydrol. Earth Syst. Sci.*, pp. 669–678, <https://doi.org/10.5194/hess-12-669-2008>, 2008.
- 460 Droogers, P., Immerzeel, W. W., and Lorite, I. J.: Estimating actual irrigation application by remotely sensed evapotranspiration observations, *Agric. Water Manag.*, 97, 1351–1359, <https://doi.org/10.1016/j.agwat.2010.03.017>, 2010.







- 500 Kim, C. P. and Stricker, J. N.: Influence of spatially variable soil hydraulic properties and rainfall intensity on the water budget, *Water Resour. Res.*, 32, 1699–1712, <https://doi.org/10.1029/96WR00603>, 1996.
- Kroes, J., van Dam, J., Bartholomeus, R., Groenendijk, P., Heinen, M., Hendriks, R., Mulder, H., Supit, I., and van Walsum, P.: SWAP version 4, Tech. rep., Wageningen University & Recharge, <https://doi.org/10.18174/416321>, <http://library.wur.nl/WebQuery/wurpubs/522980>, 2017.
- 505 Kryanova, V. and Arnold, J. G.: Advances in ecohydrological modelling with SWAT - A review, *Hydrol. Sci. J.*, 53, 939–947, <https://doi.org/10.1623/hysj.53.5.939>, 2008.
- Laio, F., Porporato, A., Fernandez-Illescas, C. P., and Rodriguez-Iturbe, I.: Plants in water-controlled ecosystems: Active role in hydrologic processes and response to water stress IV. Discussion of real cases, *Adv. Water Resour.*, 24, 745–762, [https://doi.org/10.1016/S0309-1708\(01\)00007-0](https://doi.org/10.1016/S0309-1708(01)00007-0), 2001.
- 510 Li, P. and Ren, L.: Evaluating the effects of limited irrigation on crop water productivity and reducing deep groundwater exploitation in the North China Plain using an agro-hydrological model: I. Parameter sensitivity analysis, calibration and model validation, *J. Hydrol.*, 574, 497–516, <https://doi.org/10.1016/j.jhydrol.2019.04.053>, <https://doi.org/10.1016/j.jhydrol.2019.04.053>, 2019.
- Li, Y., Grimaldi, S., Walker, J. P., and Pauwels, V. R.: Application of remote sensing data to constrain operational rainfall-driven flood forecasting: A review, <https://doi.org/10.3390/rs8060456>, 2016.
- 515 Liu, Y., Weerts, A. H., Clark, M., Hendricks Franssen, H. J., Kumar, S., Moradkhani, H., Seo, D. J., Schwanenberg, D., Smith, P., Van Dijk, A. I. J. M., Van Velzen, N., He, M., Lee, H., Noh, S. J., Rakovec, O., and Restrepo, P.: Advancing data assimilation in operational hydrologic forecasting: Progresses, challenges, and emerging opportunities, *Hydrol. Earth Syst. Sci.*, 16, 3863–3887, <https://doi.org/10.5194/hess-16-3863-2012>, 2012.
- Long, D., Longuevergne, L., and B. R. Scanlon: Uncertainty in evapotranspiration from land surface modeling, remote sensing, and GRACE satellites., *Water Resour. Res.*, 50, 1131–1151, <https://doi.org/10.1002/2013WR014581>, 2014.
- 520 Lu, Y., Steele-Dunne, S. C., and De Lannoy, G. J.: Improving soil moisture and surface turbulent heat flux estimates by assimilation of SMAP brightness temperatures or soil moisture retrievals and GOES land surface temperature retrievals, *J. Hydrometeorol.*, 21, 183–203, <https://doi.org/10.1175/JHM-D-19-0130.1>, 2020.
- Mensforth, L. J., Thorburn, P. J., Tyerman, S. D., and Walker, G. R.: Sources of water used by riparian *Eucalyptus camaldulensis* overlying highly saline groundwater, *Oecologia*, 100, 21–28, <https://doi.org/10.1007/BF00317126>, 1994.
- 525 Mitchell, H. L., Houtekamer, P. L., and Pellerin, G.: Ensemble Size, Balance, and Model-Error Representation in an Ensemble Kalman Filter\*, *Mon. Weather Rev.*, 130, 2791–2808, [https://doi.org/10.1175/1520-0493\(2002\)130<2791:ESBAME>2.0.CO;2](https://doi.org/10.1175/1520-0493(2002)130<2791:ESBAME>2.0.CO;2), 2002.
- Neumann, R. B. and Cardon, Z. G.: The magnitude of hydraulic redistribution by plant roots: a review and synthesis of empirical and modeling studies., *New Phytol.*, 194, 337–52, <https://doi.org/10.1111/j.1469-8137.2012.04088.x>, <http://doi.wiley.com/10.1111/j.1469-8137.2010.03195.x><http://www.ncbi.nlm.nih.gov/pubmed/22417121>, 2012.
- 530 Orellana, F., Verma, P., Loheide, S. P., and Daly, E.: Monitoring and modeling water-vegetation interactions in groundwater-dependent ecosystems, *Rev. Geophys.*, 50, <https://doi.org/10.1029/2011RG000383>, 2012.
- Pauwels, V. R. N. and De Lannoy, G. J. M.: Ensemble-based assimilation of discharge into rainfall-runoff models: A comparison of approaches to mapping observational information to state space, *Water Resour. Res.*, <https://doi.org/10.1029/2008WR007590>, 2009.
- 535 Pauwels, V. R. N., De Lannoy, G. J. M., Hendricks Franssen, H.-J., and Vereecken, H.: Simultaneous estimation of model state variables and observation and forecast biases using a two-stage hybrid Kalman filter, *Hydrol. Earth Syst. Sci.*, 17, 3499–3521, <https://doi.org/10.5194/hess-17-3499-2013>, <https://www.hydrol-earth-syst-sci.net/17/3499/2013/>, 2013.



- Pinheiro, E. A. R., de Jong van Lier, Q., and Šimůnek, J.: The role of soil hydraulic properties in crop water use efficiency: A process-based analysis for some Brazilian scenarios, *Agric. Syst.*, 173, 364–377, <https://doi.org/10.1016/j.agsy.2019.03.019>, 2019.
- 540 Pipunic, R. C., Ryu, D., and Walker, J. P.: Assessing Near-Surface Soil Moisture Assimilation Impacts on Modeled Root-Zone Moisture for an Australian Agricultural Landscape, *Remote Sens. Terr. Water Cycle*, 9781118872, 305–317, <https://doi.org/10.1002/9781118872086.ch18>, 2014.
- Renard, B., Kavetski, D., Kuczera, G., Thyer, M., and Franks, S. W.: Understanding predictive uncertainty in hydrologic modeling: The challenge of identifying input and structural errors, *Water Resour. Res.*, 46, 1–22, <https://doi.org/10.1029/2009WR008328>, 2010.
- 545 Scheerlinck, K., Pauwels, V. R. N., Vernieuwe, H., and De Baets, B.: Calibration of a water and energy balance model: Recursive parameter estimation versus particle swarm optimization, *Water Resour. Res.*, 45, <https://doi.org/10.1029/2009WR008051>, 2009.
- Shi, Y. and Eberhart, R.: A modified particle swarm optimizer, in: 1998 IEEE Int. Conf. Evol. Comput. Proceedings. IEEE World Congr. Comput. Intell. (Cat. No.98TH8360), pp. 69–73, IEEE, <https://doi.org/10.1109/ICEC.1998.699146>, <http://ieeexplore.ieee.org/document/699146/>, 1998.
- 550 Simmons, C. S. and Meyer, P. D.: A simplified model for the transient water budget of a shallow unsaturated zone, *Water Resour. Res.*, 36, 2835–2844, <https://doi.org/10.1029/2000WR900202>, <http://doi.wiley.com/10.1029/2000WR900202>, 2000.
- Simunek, J., Sejna, M., Saito, H., Sakai, M., and van Genuchten, M.: “The HYDRUS-1D software package for simulating the one-dimensional movement of water, heat, and multiple solutes in variably-saturated media. Version 4.08. HYDRUS Softw. Ser. 3., Dep. Environ. Sci., Univ. Calif., Riverside., p. 332, 2009.
- 555 Swaffler, B. A., Habner, N. L., Holland, K. L., and Crosbie, R. S.: Applying satellite-derived evapotranspiration rates to estimate the impact of vegetation on regional groundwater flux, *Ecohydrology*, 13, 1–14, <https://doi.org/10.1002/eco.2172>, 2020.
- Talagrand, O., Vautard, R., and Strauss, B.: Evaluation of Probabilistic Prediction Systems, Tech. rep., Meteo-France, Illkirch, France, 1997.
- Taufik, M., Setiawan, B. I., and Van Lanen, H. A.: Increased fire hazard in human-modified wetlands in Southeast Asia, *Ambio*, 48, 363–373, <https://doi.org/10.1007/s13280-018-1082-3>, <https://doi.org/10.1007/s13280-018-1082-3>, 2019.
- 560 Teuling, A. J. and Troch, P. A.: Improved understanding of soil moisture variability dynamics, *Geophysical Research Letters*, 32, <https://doi.org/10.1029/2004GL021935>, 2005.
- Therrien, R., McLaren, R., Sudicky, E., and Panday, S.: Hydrogeosphere—a three-dimensional numerical model describing fully-integrated subsurface and surface flow and solute transport., Tech. rep., Groundwater Simul. Group., Waterloo, Ont., Canada., 2006.
- van Dam, J. C., Groenendijk, P., Hendriks, R. F., and Kroes, J. G.: Advances of modeling water flow in variably saturated soils with SWAP, *Vadose Zo. J.*, 7, 640, <https://doi.org/10.2136/vzj2007.0060>, 2008.
- 565 van Genuchten, M. T.: A closed-form equation for predicting the Hydraulic conductivity of unsaturated zone, *Soil Sci. Soc. Am. J.*, 44, 892–898, 1980.
- Van Walsum, P. E. V. and Veldhuizen, A. A.: Integration of models using shared state variables: Implementation in the regional hydrologic modelling system SIMGRO, *J. Hydrol.*, 409, 363–370, <https://doi.org/10.1016/j.jhydrol.2011.08.036>, <http://dx.doi.org/10.1016/j.jhydrol.2011.08.036>, 2011.
- 570 Vrugt, J., Hopmans, J., and Simunek, J.: Calibration of a two-dimensional root water uptake model, *Soil Sci. Soc. Am. J.*, 65, 1027–1037, <https://doi.org/10.2136/sssaj2001.6541027x>, <https://dl.sciencesocieties.org/publications/sssaj/abstracts/65/4/1027>, 2001.
- Xu, X., Huang, G., Zhan, H., Qu, Z., and Huang, Q.: Integration of SWAP and MODFLOW-2000 for modeling groundwater dynamics in shallow water table areas, *J. Hydrol.*, 412–413, 170–181, <https://doi.org/10.1016/j.jhydrol.2011.07.002>, 2012.



- 575 Zeng, J., Yang, J., Zha, Y., and Shi, L.: Capturing soil-water and groundwater interactions with an iterative feedback coupling scheme : new HYDRUS package for MODFLOW, *Hydrol. Earth Syst. Sci.*, pp. 637–655, 2019.
- Zhang, H., Kurtz, W., Kollet, S., Vereecken, H., and Franssen, H. J. H.: Comparison of different assimilation methodologies of groundwater levels to improve predictions of root zone soil moisture with an integrated terrestrial system model, *Adv. Water Resour.*, 111, 224–238, <https://doi.org/10.1016/j.advwatres.2017.11.003>, <https://doi.org/10.1016/j.advwatres.2017.11.003>, 2018.
- 580 Zhu, Y., Zha, Y.-y., Tong, J.-x., and Yang, J.-z.: Method of coupling 1-D unsaturated flow with 3-D saturated flow on large scale, *Water Sci. Eng.*, 4, 357–373, <https://doi.org/10.3882/j.issn.1674-2370.2011.04.001>, <http://www.sciencedirect.com/science/article/pii/S167423701530168X>, 2011.
- Zhu, Y., Shi, L., Lin, L., Yang, J., and Ye, M.: A fully coupled numerical modeling for regional unsaturated-saturated water flow, *J. Hydrol.*, 475, 188–203, <https://doi.org/10.1016/j.jhydrol.2012.09.048>, <http://dx.doi.org/10.1016/j.jhydrol.2012.09.048>, 2012.